The actin protrusion deforms the nucleus during invasion through basement membrane

Johan d'Humières[1], Lianzijun Wang[2], David R. Sherwood[2], Julie Plastino[1*]
[1] Laboratoire de physique de l'Ecole Normale Supérieure, ENS, Université PSL, CNRS, Sorbonne Université, Université Paris Cité, F-75005 Paris, France
[2]Department of Biology, Duke University, Durham, NC 27708, USA

*Corresponding author:
Julie Plastino (julie.plastino@phys.ens.fr)

Classification: Biophysics, Developmental Biology
Keywords: actin dynamics, nuclear deformation, cell invasion, *C. elegans*

ABSTRACT

Cell invasion through basement membrane (BM) extracellular matrix barriers is important during organ development, immune cell trafficking, and cancer metastasis. Here we study an invasion event, anchor cell (AC) invasion, which occurs during *Caenorhabditis elegans* development. The actin protrusion of the invading AC mechanically displaces the BM, but it is not known how forces are balanced to prevent the growing actin protrusion from pushing itself backward when confronted with a load. Here we observe that the distal end of the actin protrusion in the invading AC abuts the nucleus and deforms it. Further we show that there is a correlation between invasion efficiency and nuclear deformation: under mutant conditions where invasion is reduced, nuclear deformation is diminished. However, nuclear deformation and invasion are unaffected by interfering with the molecular connections between the actin and microtubule cytoskeletons and the nuclear envelope. Together these data suggest that the AC actin protrusion braces against the nucleus to apply forces during invasion, but that nucleus-cytoskeleton molecular connections are not necessary for this to occur.

SUMMARY STATEMENT

Actin-based membrane protrusions in invading cells apply force to basement membrane (BM) barriers to help break through them. In cell motility in 2D, the actin protrusion uses cell-substrate adhesions for leverage to push forward against obstacles in what is known as the molecular clutch. The situation is different in 3D invasion, where the adhesive substrate is being effaced by the invading cell. It is not clear, in this case, why the growing actin protrusion doesn't push itself backwards instead of extending forwards through the BM. The data presented here provide evidence that the distal end of the invasive actin protrusion is braced against the stiff, immobile nucleus, allowing growth of the proximal end to apply force on the BM.

MAIN TEXT

INTRODUCTION

Much is known about the mechanisms of cell motility in 2D systems, including how cytoskeleton assembly at the front of the cell is transduced into whole cell motility by coupling cytoskeleton flows to adhesions in what is known as the molecular clutch (Giannone et al., 2009). However the situation is more complicated in 3D environments (Caswell and Zech, 2018; Lämmermann and Sixt, 2009). Since the vast majority of physiologically-relevant cell movements occur in a 3D context, understanding movement through extracellular matrix (ECM) in complex geometries is of broad interest in the fields of biophysics, cell and developmental biology, and also for the study of diseases such as cancer.

Indeed cancer cell invasion represents a particular mystery as concerns 3D movement as cancer cells not only attach to the matrix to pull themselves forward, but also digest and displace through physical force that very same matrix in order to make holes large enough to accommodate nuclear translocation (Ferrari et al., 2019a). Recently it has been proposed in an invasive breast cancer model that actin networks growing against positively-curved ECM collagen fibers develop shear stress in the core of the network that allows the actin protrusion to exert force on the ECM (Ferrari et al., 2019b; Infante et al., 2018). An alternative is that the invasive protrusion braces itself against the nucleus in order to push out a protrusion instead of pulling itself forward via attachments to the matrix that is being degraded. Indentations of the nucleus have been observed in invading cells that are consistent with this model (Revach and Geiger, 2014).

Here we sought to explore these different scenarios using a visually accessible in vivo 3D invasive event, anchor cell (AC) invasion in *Caenorhabditis elegans*. AC invasion occurs as part of the normal development of the *C. elegans* reproductive system, where the uterine AC generates a large opening in the underlying basement membrane (BM) to connect the uterine and vulval epithelial cell layers, a process crucial to the formation of the egg-laying apparatus of the animal (Sherwood and Sternberg, 2003). AC invasion resembles pathological cancer cell invasion in all main respects, including the dependence on actin dynamics and proteases for correct invasion (Kenny-Ganzert and Sherwood, 2024). Unlike cancer cell invasion, AC breaching of the BM is not followed by migration through the BM gap: the invasive protrusion retracts once invasion is complete, and the AC eventually fuses with its neighbors. In this way, AC invasion allows for the study of how holes are made in ECM barriers, without the confusing contribution of concomitant motility.

The AC is a small cell, and the invasive protrusion is close to the nucleus, so in this study we focused on the potential role of the nucleus in invasion. We also sought to determine the importance of the Linker of Nucleoskeleton and Cytoskeleton (LINC) complex in AC invasion. The LINC complex connects the actin and microtubule cytoskeletons to the nuclear envelope via the nesprin and SUN proteins, and hence to the lamin nucleocytoskeleton that underlies the nuclear envelope, and contributes to nuclear shape and mechanical properties in many systems (Starr and Fridolfsson, 2010).

RESULTS AND DISCUSSION

Nuclear shape and the actin protrusion

AC invasion occurs reproducibly at a specific stage of worm development that can be identified by the stereotyped divisions of the underlying vulval precursor cell (VPC) P6.p (Sherwood and Sternberg, 2003). This allows a large number of invasion events to be observed and quantitative data to be obtained from synchronized worm populations. In wild-type invasion, the AC forms a hole in the BM separating the uterine and vulval epithelial tissues between the P6.p late 2-cell stage (two daughters of P6.p) and the early 4-cell stage (four daughters of P6.p), a period of ~90 minutes (Figure 1A) (Kenny-Ganzert and Sherwood, 2024). At the early-to-mid 2-cell stage, the BM is intact and actin is beginning to accumulate at the invasive edge accompanied by BM deformation as characterized in (Cáceres et al., 2018). By the 4-cell stage, a hole as large as the AC has been created in over 98% of worms in the wild-type case (N > 100), and the actin protrusion fills the opening (Figure 1A).

During invasion we observed that the nucleus of the AC was deformed, as visualized using worm strains carrying fluorescently-labeled, endogenous nuclear lamin, introduced by CRISPR genome editing following the method reported in (Dokshin et al., 2018) and inspired by the GFP version produced in (Link et al., 2018) (Figure 1B). At earlier stages, where actin assembles in the form of foci that depress the underlying BM (Hagedorn et al., 2013), we observed that the foci corresponded to dents in the AC nuclear lamin contour, while the large invasive protrusion of later stages created substantial depressions in the nuclear envelope (Figure 1B). These were not the only phenotypes observed: in general nuclear outlines appeared to follow the shape of the actin protrusions in the AC, and as a result, the lamin contour was variously observed to be flattened, pinched or indented.

Nuclear deformation and invasion

To gain insight into the functional significance of actin-based nuclear deformation, we examined a worm strain that was null for the gene of the single homolog of the WSP-1/N-WASP protein (Withee et al., 2004). WASP is an actin polymerization activator that catalyzes the activity of the Arp2/3 complex, one of the main actin polymerization nucleation factors responsible for actin structure assembly in moving and protruding cells (Blanchoin et al., 2014). From previous work it was known that the invasive actin protrusion in the AC is much reduced in *wsp-1* null animals, and successful invasion occurs in only about 20% of 4-cell stage worms (Cáceres et al., 2018; Lohmer et al., 2016). We evaluated nuclear contours in ACs of *wsp-1* null animals that had not invaded at the 4-cell stage, and we observed that the nuclei were smoother and rounder than in the control conditions (Figure 1C). As previously observed (Cáceres et al., 2018), the size of the actin protrusion was halved in mutant ACs that had not invaded (Figure 1E). We overlaid uninvaded and control nuclear contours for a whole population of worms, and worms lacking WSP-1/N-WASP that did not display invasion at the 4-cell stage had smoother AC nuclei that superimposed more neatly than control worms, which had erratic nuclear outlines (Figure 1F). We quantified this effect using the elliptical Fourier analysis approach, as previously used to analyze irregular nuclear shapes ((Tamashunas et al., 2020) and references therein). Briefly this method fits the nuclear contour with a series of diminishing ellipses, and then outputs the EFC ratio, which characterizes how well the nuclear shape was fit by the first ellipse. As such the EFC ratio is larger for more regular shapes. Indeed, the mutant, uninvaded ACs had nuclei with an average EFC ratio that was approximately double the control AC nuclei (Figure 1G).

This result showed that both invasion and nuclear shape depended on actin, but did not inform as to whether invasion efficiency was related to nuclear deformation. To test this, we took advantage of biological variability and the fact that some *wsp-1* null worms succeeded in invading. These worms had AC protrusions that were small in size, similar to uninvaded ACs, but their nuclei were nevertheless deformed by both the invasive protrusion and the cortical actin structures in the AC (Figure 1D and E). In fact, overlay analysis and EFC ratio quantification revealed that mutant ACs that succeeded in invading had nuclei as deformed as control animals (Figure 1F and G). These data were consistent with the idea that invasion happened in those *wsp-1* animals where the little actin present was organized in such a way as to abut the nucleus, allowing a smaller amount of actin to exert enough force to break through the BM.

Does the AC nucleus need to be molecularly attached to the cytoskeleton for efficient invasion?

Given the correlation of nuclear deformation with invasion efficiency, we next wondered whether a direct molecular attachment of the nuclear envelope to the cytoskeleton via the LINC complex was important for AC invasion. In *C. elegans* there are two main nesprins, ANC-1 and UNC-83, one canonical SUN protein, UNC-84, and one gene coding for lamin LMN-1 (Starr, 2019). We first focused on nesprins, the LINC component that bridges actin or microtubule cytoskeletons to the nuclear envelope. By CRISPR we fluorescently labeled the endogenous locus of the two main *C. elegans* nesprins, *anc-1* and *unc-83*, to probe whether these proteins were expressed in the AC at the time of invasion. Both nesprins were present in the AC at the 4-cell stage, although the label was not only on the nuclear envelope, but appeared also cytoplasmic, perhaps associated with the endoplasmic reticulum (Figure 2A and B). This was especially true for UNC-83, which was overall very faint. Nuclear enrichment became more evident at later stages of vulval morphogenesis (Figure 2A and B).

Based on this, we next evaluated AC invasion at the 4-cell stage of an *anc-1* null mutant *e1873* (Starr and Han, 2002) after crossing it into a strain carrying fluorescent BM so we could unambiguously identify faulty invasion events. We observed no difference in invasion between this mutant and a control strain, both showing almost 100% invasion at the 4-cell stage (Table 1, line 2 compared to line 1). To address possible redundancy of nesprins, we further knocked down *unc-83* by RNAi feeding in the *anc-1* null mutant background, and we observed a trend toward more failed invasion although the difference with control animals was of borderline significance ($p = 0.05$, Table 1, line 3 compared to line 1). Following up on this, we took a dominant negative approach to reducing nesprin function in the AC, and expressed the KASH domain, as has been developed and extensively used in mammalian cells to block nesprin function (Lombardi et al., 2011; Stewart-Hutchison et al., 2008). Overexpression of the KASH domain saturates all the SUN binding sites on the nuclear envelope, displacing nesprin and thereby rupturing the nucleus-cytoskeleton link. We saw no effect on invasion when KASH was expressed in the AC (Table 1, line 4). We crossed this KASH strain into the strain carrying fluorescently-labeled nuclei and F-actin (used in Figure 1B), and observed that fluorescent KASH was enriched on the AC nucleus as expected although also present in the cytoplasm due to overexpression (Figure 2C). Nevertheless the nuclei appeared indented by the invasive actin protrusion as observed in control animals (Figure 2C versus Figure 1B), and the EFC ratio was comparable (Figure 2D). This result indicated that KASH overexpression, presumably disconnecting the nucleus from the cytoskeleton, had no effect on invasion or how the actin protrusion deformed the nucleus during invasion.

AC invasion is a robust process, and sometimes compensating mechanisms mask the functional consequences of applied perturbations. This was the case, for example, with matrix metalloproteases (MMPs), the removal of which on their own had no effect on AC invasion at the 4-cell stage (Kelley et al., 2019). However, when combined with perturbations of actin assembly, the lack of MMPs became deleterious for AC invasion, and it was revealed that actin was upregulated in the AC when proteases were not present, making a bigger protrusion that succeeded in breaking the BM without digestion by proteases. With this in mind, we tried sensitizing the KASH strain by inhibiting actin assembly (*arx-2* RNAi) and interfering with proteases (crossing with worms lacking MMPs, called MMP-), but found no additional invasion defect as compared to the treatments on their own (Table 1, compare lines 5 and 6 for *arx-2* RNAi, and lines 7 and 8 for MMP-). In keeping with this and the lack of effect of RNAi against *unc-83*, the nesprin implicated in linking the microtubule cytoskeleton to the nuclear envelope (Starr, 2019), RNAi knock-down of tubulin (*tba-2*) had no effect on AC invasion.

Switching our focus away from nesprin perturbation, we next targeted nuclear lamin, to test if altering the most upstream component of the LINC complex would reveal effects that were otherwise masked by compensation and protein redundancies. However knocking down lamin in a control strain (Table 1, line 10) or even in the sensitized MMP- background (Table 1, line 11) showed no significant difference in the efficiency of AC invasion at the 4-cell stage as compared to invasion in the respective strains in the absence of RNAi. Consistent with this, there was no difference in AC nucleus EFC ratio in *lmn-1* RNAi conditions as compared to control animals, evaluated by performing RNAi in a strain carrying fluorescent nuclear pores (Thomas et al., 2023) to enable nuclear contour visualization in the absence of lamin (Figure 2D and E). Taken together these experiments broadly targeting different components of the LINC complex offer compelling evidence that the molecular attachment of the cytoskeleton to the nucleus is not required for AC invasion.

Conclusion

All together the data presented here are consistent with the invasive protrusion pushing off of the nucleus in order to break through the BM. We took advantage of the phenotypic diversity of the WSP-1/N-WASP deleted mutant to parse out cause and effect: the lack of nuclear deformation was not just due to reduced F-actin in the AC, as cells sometimes invaded (deformed nuclei) or did not (undeformed nuclei) although in both cases accumulation of F-actin at the invasive edge was reduced. This result showed that a suboptimal amount of actin, when organized properly to abut and deform the nucleus, is sufficient to assure invasion.

In this context it is important to note that polymerization of actin networks in cells can produce 1 to 10 kPa of force, depending on cell type (Abraham et al., 1999; Brunner et al., 2006), and that we have previously reported that the AC exerts about 30 nN on the BM (Cáceres et al., 2018), which translates to kPa range of forces depending on the protrusion size. Nuclei have an average elastic modulus in about the same range (Fisher et al., 2020; Krause et al., 2013; Liu et al., 2014) so it is reasonable to suggest that the actin protrusion deforms the nucleus.

Somewhat surprisingly we found no functional role for a molecular connection via the LINC complex between the AC cytoskeleton and the nucleus. However it has been shown in other systems that force transmission to the nucleus can occur independently of the LINC complex when actin networks are pushed up against the nucleus by geometrical confinement (Thiam et al., 2016). Another surprise was the fact that lamin knock-down did not affect invasion or

nuclear deformability. Lamin is generally believed to be one of the main determinants of nuclear mechanical properties, and reducing lamin softens nuclei, making them more deformable (Vahabikashi et al., 2022). However this effect may depend on cell type as RNAi against *lmn-1* in *C. elegans* makes the nuclei muscle and hypodermal cells more deformable, but neuronal cell nuclei are unaffected (Zuela-Sopilniak et al., 2020; Zuela et al., 2016). Lamin is, after all, not the only thing that contributes to nuclear stiffness. Chromatin and its compaction state, i.e., the balance between euchromatin and heterochromatin, also contribute to defining nuclear mechanics (Stephans et al., 2017; Stephans et al., 2018).

Overall we conclude that the AC braces its actin protrusion against the nucleus to apply force to the BM and invade it.

FIGURE LEGENDS

Figure 1 Nuclear shape and the actin protrusion. A) AC invasion progression from the P6.p 2-cell stage, uninvaded stage to the 4-cell stage where invasion is complete, as visualized by the hole in BM fluorescence (yellow arrowheads). Invasion is wild-type in these control worms. DIC coupled with mCherry-labeled laminin (BM) and GFP-labeled Lifeact (F-actin). **B)** Invasive actin structures (red arrowheads) deform the AC nucleus (yellow arrowheads) at both the 2-cell and the 4-cell stage in control worms displaying wild-type invasion. Lifeact-GFP and tagRFP-T-lamin. **C)** and **D)** Worms carrying a null mutation in the WSP-1/N-WASP gene *wsp-1*. In most cases **C)**, the AC does not invade by the 4-cell stage (intact BM indicated by yellow arrowheads in DIC), although there are some **D)** that manage (disrupted BM indicated by yellow arrowheads in DIC). In the former case, nuclei appear smooth and round, while in the latter case, nuclei are deformed like for control animals. Lifeact-GFP and tagRFP-T-lamin. **E)** F-actin protrusion area at the 4-cell stage for control, invaded ACs, and *wsp-1* mutant ACs, both not invaded and invaded. Areas are measured on the plane where the area is maximal. **F)** Overlays of nuclear contours at the 4-cell stage for control, invaded AC nuclei, and *wsp-1* mutant AC nuclei, both not invaded and invaded. All contours are oriented with the invasive front of the AC towards the bottom. **G)** EFC ratios to evaluate nuclear shape irregularity for the contours shown in **F)**. The nuclei of mutant, uninvaded ACs are significantly smoother than those of invaded control ACs and invaded mutant ACs. **A)** is epifluorescence microscopy, **B), C)** and **D)** are single plane images obtained by spinning disk microscopy. The hemispheric plane is shown, i.e. the one with the largest footprint of the nucleus and the protrusion. All scale bars 5 μm. $N \geq 16$ for all observations. p values calculated by Student t-test.

Figure 2 Probing the molecular attachment between the AC nucleus and the cytoskeleton. A) Fluorescent labeling of the endogenous full-length ANC-1/Nesprin-1/2 by CRISPR shows that ANC-1 is expressed in the AC at the time of invasion (4-cell stage) and concentrated on the nuclear envelope at the slightly later 8-cell stage (yellow arrowheads). DIC coupled with single plane spinning disk images of GFP-ANC-1. **B)** Fluorescent labeling of the endogenous full-length UNC-83/Nesprin-4/KASH5 by CRISPR shows that UNC-83 is expressed in the AC at the time of invasion (4-cell stage) and enriched on the nuclear envelope at the slightly later 8-cell stage (yellow arrowheads). DIC coupled with single plane spinning disk images of GFP-UNC-83. **C)** The dominant negative KASH construct is expressed under an AC promotor, and is enriched at the nuclear envelope as indicated on the linescan (N.E.) drawn from the inside (green arrowhead) to the outside of the nucleus (red arrowhead). KASH-bearing nuclei are deformed by the actin protrusion like in control animals (panels in **C)** and EFC ratio in **D)**. Single plane spinning disk images of KASH-BFP, Lifeact-GFP and tagRFP-T-lamin. **E)** Nuclear lamin is knocked down by RNAi (on average 70% reduction in LMN-1 at the nuclear envelope as assessed in a tagRFP-T-lamin strain), and nuclear contours were visualized in a strain carrying fluorescent nuclear pores (NPP-21::GFP, yellow arrowhead). RNAi against *lmn-1* had no effect on nuclear deformation as quantified by EFC ratio analysis **D)**. DIC coupled with single plane spinning disk images of GFP-NPP-21/TPR (translocated promoter region). In all cases the hemispheric plane is shown, i.e. the one with the largest footprint of the nucleus and the protrusion. All scale bars 5 μm.

Figure 1

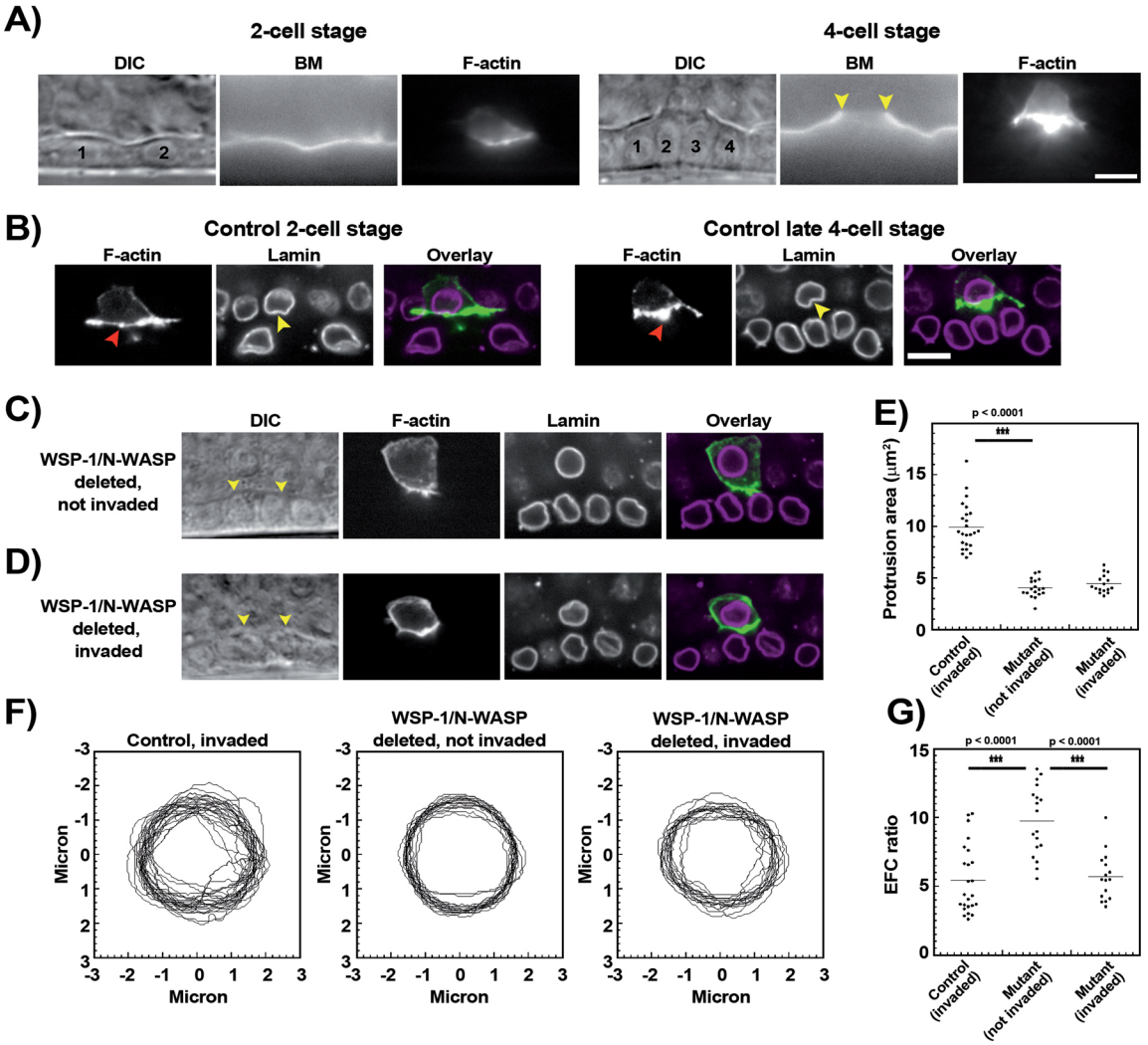
A)
2-cell stage
DIC
BM
F-actin
1
2
4-cell stage
DIC
BM
F-actin
1
2
3
4
B)
Control 2-cell stage
F-actin
Lamin
Overlay
Control late 4-cell stage
F-actin
Lamin
Overlay
C)
DIC
F-actin
Lamin
Overlay
WSP-1/N-WASP deleted, not invaded
D)
WSP-1/N-WASP deleted, invaded
E)
p < 0.0001
***
Protrusion area (μm²)
0
5
10
15
Control (invaded)
Mutant (not invaded)
Mutant (invaded)
F)
Control, invaded
WSP-1/N-WASP deleted, not invaded
WSP-1/N-WASP deleted, invaded
Micron
-3
-2
-1
0
1
2
3
G)
p < 0.0001
***
p < 0.0001
***
EFC ratio
0
5
10
15
Control (invaded)
Mutant (not invaded)
Mutant (invaded)

Figure 2

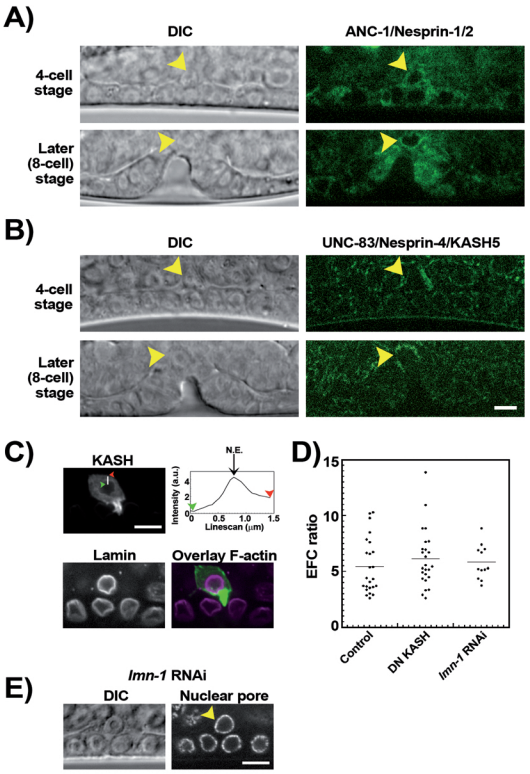
A)
DIC
ANC-1/Nesprin-1/2
4-cell stage
Later (8-cell) stage
B)
DIC
UNC-83/Nesprin-4/KASH5
4-cell stage
Later (8-cell) stage
C)
KASH
N.E.
Intensity (a.u.)
Linescan (μm)
Lamin
Overlay F-actin
D)
EFC ratio
Control
DN KASH
lmn-1 RNAi
E)
lmn-1 RNAi
DIC
Nuclear pore

Table 1: Evaluation of AC invasion at the 4-cell stage in different mutant and RNAi conditions.

Line #	Genotype (Worm strain name)	RNAi treatment	% full invasion (# of worms)	% partial or no invasion (# of worms)	N
1	*qyIs127 [Plam-1::lam-1::mCherry]; qyIs242 [Pcdh-3::Lifeact::GFP]* (JUP60)	None (L4440 control)	98%[a,b] (61)	2% (1)	62
2	*anc-1(e1873) I; qyIs127 [Plam-1::lam-1::mCherry]* (JUP116)	None (L4440 control)	96% (26)	4% (1)	27
3	*anc-1(e1873) I; qyIs127 [Plam-1::lam-1::mCherry]* (JUP116)	*unc-83* RNAi	89%[a] (48)	11% (6)	54
4	*sybIs5165 [Pzmp-1-pes-10-BFP-KASH]; qyIs127 [Plam-1::lam-1::mCherry]; qyIs242 [Pcdh-3::Lifeact::GFP]* (JUP124)	None	97% (56)	3% (2)	58
5	*qyIs127 [Plam-1::lam-1::mCherry]; qyIs242 [Pcdh-3::Lifeact::GFP]* (JUP60)	*arx-2* RNAi	66%[b,c] (52)	34% (27)	79
6	*sybIs5165 [Pzmp-1-pes-10-BFP-KASH]; qyIs127 [Plam-1::lam-1::mCherry]; qyIs242 [Pcdh-3::Lifeact::GFP]* (JUP124)	*arx-2* RNAi	56%[c] (47)	44% (37)	84
7	*sybIs5165 [Pzmp-1-pes-10-BFP-KASH]; qyIs127 [Plam-1::lam-1::mCherry]; qyIs242 [Pcdh-3::Lifeact::GFP] ; zmp-1(cg115) III; zmp-6 (tm3073) III* (NK3141)	None	72%	28%	53
8	*qyIs127 [Plam-1::lam-1::mCherry]; qyIs242 [Pcdh-3::Lifeact::GFP] ; zmp-1(cg115) III; zmp-6 (tm3073) III* (JUP65)	None	73%[d]	27%	51
9	*lmn-1(jf98[lmn-1::GFP])* (UV117)[e]	*tba-2* RNAi	100% (21)	0% (0)	21
10	*qyIs127 [Plam-1::lam-1::mCherry]; qyIs242 [Pcdh-3::Lifeact::GFP]* (JUP60)	*lmn-1* RNAi	95% (18)	5% (1)	19
11	*qyIs127 [Plam-1::lam-1::mCherry]; qyIs242 [Pcdh-3::Lifeact::GFP] ; zmp-1(cg115) III; zmp-6 (tm3073) III* (JUP65)	*lmn-1* RNAi	67%[d] (30)	33% (15)	45

p values for Chi-squared significance tests: [a] $p = 0.05$, [b] $p < 0.0001$, [c] $p = 0.2$, [d] $p = 0.5$

[e] UV117 is a CRISPR GFP-LMN-1 strain that displayed wild-type invasion.

MATERIALS AND METHODS

Constructs, alleles and worm strains

The alleles *qyIs127 [Plam-1::lam-1::mCherry]*, *qyIs242 [Pcdh-3::Lifeact::GFP]*, *zmp-1(cg115)* III and *zmp-6 (tm3073) III* are described in previous studies (Cáceres et al., 2018; Kelley et al., 2019). The *anc-1(e1873)* I (strain CB3440) and *wsp-1(gm324)* IV (strain NG324) were provided by the *Caenorhabditis* Genetics Center. CRISPR/CAS9-genome edited strain *lmn-1(jf98[lmn-1::GFP])* I (strain UV117) was a kind gift from Verena Jantsch (Link et al., 2018) and CRISPR/CAS9-genome edited strain *npp-21 bq1[npp-21::gfp]); bqSi189[pBN13(unc-119(+) lmn-1p::mCherry::his-58)]* II (strain BN1062) was a kind gift from Peter Askjaer (Thomas et al., 2023).

CRISPR/CAS9-genome edited *anc-1 (bab341 [mEGFP::anc-1a])* I (strain MCP341), *unc-83 (bab346 [mEGFP::unc-83])* I (strain MCP346) and *lmn-1 (bab344 [tagRFP::lmn-1])* I (strain MCP344) were generated at the SEGiCel facility (Université Lyon 1, UMS3421, Lyon, France). For *anc-1a* and *unc-83a*, the longest, full-length forms were labeled on their N-terminus with a monomeric form of enhanced GFP containing a syntron, followed by GASGASGAS linker before the start ATG. For *lmn-1*, tagRFP-T with syntrons followed by the linker ASLYKKAGS was introduced on the N-terminus of the gene coding for LMN-1. Oligonucleotide sequences used to create these strains are detailed in Supplementary Table 1.

The gene for the dominant negative KASH construct (for allele *sybIs5165*) was synthesized by Eurofins and consisted of the tag-BFP gene with syntrons followed by a GGSGGGSGG linker and then the neck region, transmembrane domain and the luminal domain of ANC-1 as defined in (Hao et al., 2021). This construct was recombined into Gateway cloning vector pDONR221. The promoter sequence *Pzmp-1* and the enhancer element *pes-10* were amplified from *pBS-zmp-1p-pes-10-spGFP1-10* as done in (Hagedorn et al., 2009), and introduced into Gateway cloning vector pDONR[P4-P1R]. The entry vectors were recombined along with the *unc-54 3'UTR* (gift of G. Seydoux; Addgene plasmid #17253: pCM5.37) into the destination vector pCFJ150 - pDESTttTi5605[R4-R3] (gift from Erik Jorgensen Addgene plasmid # 19329). The construct was injected into DP38 *unc-119(ed3)* and integrated by Suny Biotech. The strain was outcrossed at least twice before use.

Crossing different alleles gave the worm strains indicated in Table 1, and also JUP138 *qyIs242 [Pcdh-3::Lifeact::GFP]*; *lmn-1(bab344 [tagRFP::lmn-1]* I and JUP139 *wsp-1(gm324)* IV; *qyIs242 [Pcdh-3::Lifeact::GFP]*; *lmn-1(bab344 [tagRFP::lmn-1]* I.

RNAi treatment

Strains were grown at room temperature on agar plates containing NGM growth media and seeded with *Escherichia coli* OP50 strain. Worms were synchronized by bleach and starved to arrest at the L1 stage, and then fed OP50 at room temperature until AC invasion was scored. RNAi was performed by feeding bacteria producing target dsRNAs to larvae at room temperature. Phenotypes were scored at the 4-cell stage. Empty L4440 was used as a negative control. Probes for *arx-2* and *tba-2* were obtained from the Vidal ORF RNAi library (Rual et al., 2004). Probes for *unc-83* and *lmn-1* were obtained from the Ahringer RNAi library distributed by Source Bioscience (Kamath and Ahringer, 2003).

Imaging

Worms were anesthetized in 30 µL of 10 mM (0.2%) levamisole for 10-15 min, and then mounted on 4.5% noble agar pads. Samples were sealed with melted VALAP (vaseline,

lanolin, paraffin 1:1:1 w/w/w). Image acquisition was performed at room temperature with an upright confocal spinning disk microscope from Roper/Zeiss using a 100x 1.46 OIL DIC ALPHA PL APO (UV) VIS-IR objective and a CoolSNAP HQ2 camera controlled by Metamorph software. DIC optics were used and laser lines at 405 nm, 491 nm and 561 nm. For z-stacks the step size was 0.2 μm. All wavelengths were acquired at each z slice in order to correlate actin structures with lamin dents and wrinkles.

EFC ratio analysis

Masks for nuclear contours were made by thresholding in Metamorph. These masks were fed into a custom Matlab script, a kind gift of Alice Williart (Matthieu Piel laboratory, Institut Curie) based on the original script developed in (Tamashunas et al., 2020). The number of harmonics, N, was taken as 25.

Statistical analysis

For comparison of % phenotypes with RNAi, a chi-squared test was employed. Other data is represented as dot-plots, and data was compared using a Student t-test. In all cases the resulting p values are reported in the figures or in the table footnotes. $p < 0.05$ is taken as significant.

ACKNOWLEDGEMENTS

Spinning disk imaging was performed at the Cell and Tissue Imaging Platform (member of France–BioImaging, ANR-10-INBS-04) of the Genetics and Developmental Biology Department (UMR3215/U934) of Institut Curie. Some worm strains were obtained from the *Caenorhabditis* Genetics Center, which is funded by NIH Office of Research Infrastructure Programs (P40 OD010440). All the CRISPR strains made in this study were generated by SEGiCel (SFR Santé Lyon Est CNRS UAR 3453, Lyon, France) with the support of CNRS and IBiSA. D.R.S. acknowledges financial support by the National Institutes of Health (Grant R35GM118049). JdH acknowledges the Ministère de l'Enseignement Supérieur et de la Recherche for PhD funding. J.P. acknowledges financial support from the Fondation ARC (Grant PJA 20191209604) and the Human Frontiers Science Program Organization (Grant RGP0026/2020).

DISCLOSURES

The authors declare that they have no conflicts of interest with the contents of this article.

REFERENCES

Abraham, V.C., V. Krishnamurthi, D.L. Taylor, and F. Lanni. 1999. The actin-based nanomachine at the leading edge of migrating cells. *Biophys. J.* 77:1721-1732.

Blanchoin, L., R. Boujemaa-Paterski, C. Sykes, and J. Plastino. 2014. Actin dynamics, architecture and mechanics in cell motility. *Physiol. Rev.* 94:235-263.

Brunner, C.A., A. Ehrlicher, B. Kohlstrunk, D. Knebel, J.A. Käs, and M. Goegler. 2006. Cell migration through small gaps. *Eur. Biophys. J.* 35:713-719.

Cáceres, R., N. Bojanala, L.C. Kelley, J. Dreier, J. Manzi, F. Di Federico, Q. Chi, T. Risler, I. Testa, D.R. Sherwood, and J. Plastino. 2018. Forces drive basement membrane invasion in *Caenorhabditis elegans*. *Proc. Natl. Acad. Sci. U.S.A.* 115:11537–11542.

Caswell, P.T., and T. Zech. 2018. Actin-based cell protrusion in a 3D matrix. *Trends Cell Biol.* 28:823-834.

Dokshin, G.A., K.S. Ghanta, K.M. Piscopo, and C.C. Mello. 2018. Robust genome editing with short single-stranded and long, partially single-stranded DNA donors in *Caenorhabditis elegans*. *Genetics*. 210:781-787.

Ferrari, R., E. Infante, and P. Chavrier. 2019a. Nucleus–invadopodia duo during cancer invasion. *Trends Cell Biol.* 29:93-96.

Ferrari, R., G. Martin, O. Tagit, A. Guichard, A. Cambi, R. Voituriez, S. Vassilopoulos, and P. Chavrier. 2019b. MT1-MMP directs force-producing proteolytic contacts that drive tumor cell invasion. *Nat. Commun.* 10:4886.

Fisher, T., A. Hayn, and C.T. Mierke. 2020. Effect of nuclear stiffness on cell mechanics and migration of human breast cancer cells. *Front. Cell Dev. Biol.* 8:393.

Giannone, G., R.-M. Mège, and O. Thoumine. 2009. Multi-level molecular clutches in motile cell processes. *Trends Cell Biol.* 19:475-486.

Hagedorn, E.J., H. Yashiro, J.W. Ziel, S. Ihara, Z. Wang, and D.R. Sherwood. 2009. Integrin Acts Upstream of Netrin Signaling to Regulate Formation of the Anchor Cell's Invasive Membrane in C. elegans. *Dev. Cell*. 17:187-198.

Hagedorn, E.J., J.W. Ziel, M.A. Morrissey, L.M. Linden, Z. Wang, Q. Chi, S.A. Johnson, and D.R. Sherwood. 2013. The netrin receptor DCC focuses invadopodia-driven basement membrane transmigration in vivo. *J. Cell Biol.* 201:903-913.

Hao, H., S. Kalra, L.E. Jameson, L.A. Guerrero, N.E. Cain, J. Bolivar, and D.A. Starr. 2021. The Nesprin-1/-2 ortholog ANC-1 regulates organelle positioning in C. elegans independently from its KASH or actin-binding domains. *eLife*. 10:e61069.

Infante, E., A. Castagnino, R. Ferrari, P. Monteiro, S. Agüera-González, P. Paul-Gilloteaux, M.J. Domingues, P. Maiuri, M. Raab, C.M. Shanahan, A. Baffet, M. Piel, E.R. Gomes, and P. Chavrier. 2018. LINC complex-Lis1 interplay controls MT1-MMP matrix digest-on-demand response for confined tumor cell migration. *Nat. Commun.* 9:2443.

Kamath, R.S., and J. Ahringer. 2003. Genome-wide RNAi screening in Caenorhabditis elegans. *Methods*. 30:313-321.

Kelley, L.C., Q. Chi, R. Cáceres, E. Hastie, A.J. Schindler, Y. Jiang, D.Q. Matus, J. Plastino, and D.R. Sherwood. 2019. Adaptive F-actin polymerization and localized ATP production drive basement membrane invasion in the absence of MMPs. *Dev. Cell*. 48:313-328.

Kenny-Ganzert, I.W., and D.R. Sherwood. 2024. The *C. elegans* anchor cell: A model to elucidate mechanisms underlying invasion through basement membrane. *Sem. Cell Dev. Biol.* 154:23-34.

Krause, M., J. te Riet, and K. Wolf. 2013. Probing the compressibility of tumor cell nuclei by combined atomic force–confocal microscopy. *Phys. Biol.* 10:065002.

Lämmermann, T., and M. Sixt. 2009. Mechanical modes of 'amoeboid' cell migration. *Curr. Opin. Cell Biol.* 21:636-644.

Link, J., D. Paouneskou, M. Velkova, A. Daryabeigi, T. Laos, S. Labella, C. Barroso, S.P. Piñol, A. Montoya, H. Kramer, A. Woglar, A. Baudrimont, S.M. Markert, C. Stigloher, E. Martinez-Perez, A. Dammermann, M. Alsheimer, M. Zetka, and V. Jantsch. 2018. Transient and partial nuclear lamina disruption promotes chromosome movement in early meiotic prophase. *Dev. Cell*. 45:212-225.

Liu, H., J. Wen, Y. Xiao, J. Liu, S. Hopyan, M. Radisic, C.A. Simmons, and Y. Sun. 2014. In situ mechanical characterization of the cell nucleus by atomic force microscopy. *ACS Nano*. 8:3821-3828.

Lohmer, L.L., M.R. Clay, K.M. Naegeli, Q. Chi, J.W. Ziel, E.J. Hagedorn, J.E. Park, R. Jayadev, and D.R. Sherwood. 2016. A sensitized screen for genes promoting invadopodia function in vivo: CDC-42 and Rab GDI-1 direct distinct aspects of invadopodia formation. *PLOS Genetics*. 12:e1005786.

Lombardi, M.L., D.E. Jaalouk, C.M. Shanahan, B. Burke, K.J. Roux, and J. Lammerding. 2011. The interaction between Nesprins and Sun Proteins at the nuclear envelope is critical for force transmission between the nucleus and cytoskeleton. *J. Biol. Chem.* 286:26743-26753.

Revach, O.-Y., and B. Geiger. 2014. The interplay between the proteolytic, invasive, and adhesive domains of invadopodia and their roles in cancer invasion. *Cell Adh. Migr.* 8:215-225.

Rual, J.F., J. Ceron, J. Koreth, T. Hao, A.S. Nicot, T. Hirozane-Kishikawa, J. Vandenhaute, S.H. Orkin, D.E. Hill, S. van den Heuvel, and M. Vidal. 2004. Toward improving *Caenorhabditis elegans* phenome mapping with an ORFeome-based RNAi library. *Genome Res.* 14:2162-2168.

Sherwood, D.R., and P.W. Sternberg. 2003. Anchor cell invasion into the vulval epithelium in *C. elegans*. *Dev. Cell*. 5:21-31.

Starr, D.A. 2019. A network of nuclear envelope proteins and cytoskeletal force generators mediates movements of and within nuclei throughout *Caenorhabditis elegans* development. *Exp. Biol. Med.* 244:1323-1332.

Starr, D.A., and H.N. Fridolfsson. 2010. Interactions between nuclei and the cytoskeleton are mediated by SUN-KASH nuclear-envelope bridges. *Annu. Rev. Cell Dev. Biol.* 26:421-444.

Starr, D.A., and M. Han. 2002. Role of ANC-1 in tethering nuclei to the actin cytoskeleton. *Science*. 298:406-409.

Stephans, A.D., E.J. Banigan, S.A. Adam, R.D. Goldman, and J.F. Marko. 2017. Chromatin and lamin A determine two different mechanical response regimes of the cell nucleus. *Mol. Biol. Cell*. 28:1984-1996.

Stephans, A.D., E.J. Banigan, and J.F. Marko. 2018. Separate roles for chromatin and lamins in nuclear mechanics. *Nucleus*. 9:119-124.

Stewart-Hutchison, P.J., C.M. Hale, D. Wirtz, and D. Hodzic. 2008. Structural requirements for the assembly of LINC complexes and their function in cellular mechanical stiffness. *Exp. Cell Res.* 314:1892-1905.

Tamashunas, A.C., V.J. Tocco, J. Matthews, Q. Zhang, K.R. Atanasova, L. Paschall, S. Pathak, R. Ratnayake, A.D. Stephens, H. Luesch, J.D. Licht, and T.P. Lele. 2020. High-throughput gene screen reveals modulators of nuclear shape. *Mol. Biol. Cell*. 31:1392-1402.

Thiam, H.-R., P. Vargas, N. Carpi, C.L. Crespo, M. Raab, E. Terriac, M.C. King, J. Jacobelli, A.S. Alberts, T. Stradal, A.-M. Lennon-Dumenil, and M. Piel. 2016. Perinuclear

Arp2/3-driven actin polymerization enables nuclear deformation to facilitate cell migration through complex environments. *Nat. Commun.* 7:10997.

Thomas, L., B.T. Ismail, P. Askjaer, and G. Seydoux. 2023. Nucleoporin foci are stress-sensitive condensates dispensable for *C. elegans* nuclear pore assembly. *EMBO J.* 42:e112987.

Vahabikashi, A., S. Sivagurunathan, F.A. Sadsad Nicdao, Y.L. Han, C.Y. Park, M. Kittisopikul, X. Wong, J.R. Tran, G.G. Gundersen, K.L. Reddy, G.W.G. Luxton, M. Guo, J.J. Fredberg, Y. Zheng, S.A. Adam, and R.D. Goldman. 2022. Nuclear lamin isoforms differentially contribute to LINC complex-dependent nucleocytoskeletal coupling and whole-cell mechanics. *Proc. Natl. Acad. Sci.* 119:e2121816119.

Withee, J., B. Galligan, N. Hawkins, and G. Garriga. 2004. *Caenorhabditis elegans* WASP and Ena/VASP protiens play compensatory roles in morphogenesis and neuronal cell migration. *Genetics*. 167:1165-1176.

Zuela-Sopilniak, N., D. Bar-Sela, C. Charar, O. Wintner, and Y. Gruenbaum. 2020. Measuring nucleus mechanics within a living multicellular organism: physical decoupling and attenuated recovery rate are physiological protective mechanisms of the cell nucleus under high mechanical load. *Mol. Biol. Cell*. 31:1943-1950.

Zuela, N., M. Zwerger, T. Levin, O. Medalia, and Y. Gruenbaum. 2016. Impaired mechanical response of an EDMD mutation leads to motility phenotypes that are repaired by loss of prenylation. *J. Cell Sci.* 129:1781-1791.

SUPPLEMENTARY TABLE 1: Oligo sequences used to generate the CRISPR strains.

Name	Sequence 5'→ 3'	Function
Project: *anc-1 (bab341 [mEGFP::anc-1a])* I		
crRNA NB032	ggtcATGTCGAGCTCTCCTC-CGG	DNA sequence of RNA guide
oNB268	ATGGTGTCAAAGGGAGAAGAG	Forward primer mEGFP with start codon
oNB269	acctccagatccacctccggaacctccCTTGTAGAGCTCGTCCATTCC	Reverse primer mEGFP + linker
oNB274	gaggtctttctgtttccagagaccacctataaacacaacaaaacaatacacgtcttccgacccactaacttttttatattactaggtctaatataggtcATGGTGTCAAAGGGAGAAGAG	Forward primer for repair with homologous arms
oNB275	ttgagattttctggatttctagattttcacaatatctcaaacttacGTGGTCTAAACCTGAAGCAGACGCAGCAAGGTCTAGCaGGAGGAGAGCTCGACATacctccagatccacctccg	Reverse primer for repair with homologous arms
Project: *unc-83 (bab346 [mEGFP::unc-83])* I		
crRNA NB031	caggttacgaATGGACGTAA-TGG	DNA sequence of RNA guide
oNB268	ATGGTGTCAAAGGGAGAAGAG	Forward primer mEGFP with start codon
oNB269	acctccagatccacctccggaacctccCTTGTAGAGCTCGTCCATTCC	Reverse primer mEGFP + linker
oNB270	caccctaccagtacagtatcccacgtctggatacaaacttctctgatttttttatttttattcctggacaccgaaagtaacccgaaaacaggttacgaATGGTGTCAAAGGGAGAAGAG	Forward primer for repair with homologous arms
oNB271	ttttcgtaaaatttaaagctctgcctcacCTTCAAAAGATGGTCCTCCGATGATATATCATTGGGCATCTCGACCTCCGAGAATGAGTCCATTACGTCCATacctccagatccacctccg	Reverse primer for repair with homologous arms
Project: *lmn-1 (bab344 [tagRFP::lmn-1])* I		
crRNA NB031	agaaaaATGTCATCTCGTAA-AGG	DNA sequence of RNA guide
oNB039	ATGGTCTCCAAGGGAGAGGAG	Forward primer tagRFP with start codon
oNB284	GGAGCCTGCTTTTTTGTACAAACTTGCCTTGTAGAGCTCGTCCATTCC	Reverse primer tagRFP + linker
oNB286	gtggcgcctatgacgtttcctctcttctcttacatctctctttgtctatttctgaaactaaatccaatataattaacttcttcagaaagcagcgagaaaaATGGTCTCCAAGGGAGAGGAG	Forward primer for repair with homologous arms

oNB287	ATGAATCGTCGCCTCCTCCATTGTTGCTTAGCGACGAATTCGCTGAGCGCTCTAGCGTAACAATACGAGAACTACGAGTACCTTTgCGgGAaGACATGGAGCCTGCTTTTTTGTACAAAC	Reverse primer for repair with homologous arms